Measurement of CO_2 Solubility in Ionic Liquids: [BMP][TfO] and [P14,6,6,6][Tf_2N] by Measuring Bubble-Point Pressure

Ha Na Song,[†] Byung-Chul Lee,[‡] and Jong Sung Lim*,[†]

Department of Chemical and Biomolecular Engineering, Sogang University, 1 Sinsu-Dong, Mapo-Gu, Seoul, Korea, and Department of Chemical Engineering and Nano-Bio Technology, Hannam University, 461-6 Jeonmin-dong, Yuseong-gu, Daejeon 305-811, South Korea

Solubility data of carbon dioxide (CO_2) in ionic liquids 1-butyl-1-methylpyrrolidinium trifluoromethanesulfonate ([BMP][TfO]) and trihexyltetradecylphosphonium bis(trifluoro-methylsulfonyl)imide ([P14,6,6,6][Tf_2N]) are presented at pressures up to about 70 MPa and at temperatures between (303.15 and 373.15) K. The solubility of CO_2 in ionic liquids was measured by using a high-pressure variable-volume view cell. At high CO_2 concentrations in ionic liquids, the equilibrium pressure increased very steeply. The solubility of CO_2 in the ionic liquids decreased with increasing temperature. The experimental data for the CO_2 + ionic liquid system were correlated using the Peng−Robinson equation of state.

Introduction

In the broad sense, the term "ionic liquid" includes all molten salts like a sodium chloride. (Sodium chloride's melting point is higher than 1073.15 K.) However, these days, it refers to liquids composed entirely of ions that are fluid around or below 373.15 K. Many have literally no vapor pressure, no flammability, high thermal stability, a wide liquid range, electric conductivity, and favorable solvating properties for diverse compounds. Therefore, these advantages of ionic liquids receive great attention in various chemical industries such as the green solvent industry.[1]

Ionic liquids are attracting increasing attention in many fields. Until now, a number of papers have been published about synthesizing[2,3] ionic liquids or the application of ionic liquids in many ways. Zein El Abedin and co-workers investigated the use of ionic liquids for electrical deposition.[4,5] Recent work has shown that ionic liquids are used in membrane-based systems for separation[6] and liquid−liquid separation.[7] Also, ionic liquids can serve as solvents for biocatalysts.

Ionic liquid/CO_2 solutions are important in the recovery of solutes in supercritical fluid extraction.[8] For these processes, to choose effective ionic liquids for separation, it is important to know the solubility of gas in the ionic liquid in which we want to use it. Supercritical carbon dioxide ($scCO_2$) is the most widely used solvent in various supercritical fluid industries; for example, polymer manufacturing produces the decaffeination of coffee beans, wastewater treatment, solvents for extraction, and so on.[9] This is due to its nonflammability, nontoxicity, nonpolarity, low critical temperature and pressure values, and its low price. As green solvents, the $scCO_2$ ionic liquids are used in a lot of separation processes.[10]

The purpose of this work is to know the phase behavior of CO_2 in ionic liquids. We measured the solubility of CO_2 in the ILs 1-butyl-1-methylpyrrolidinium trifluoromethanesulfonate ([BMP][TfO]) and trihexyltetradecylphosphonium bis(trifluoromethylsulfonyl)imide ([P14,6,6,6][Tf_2N]). The range of temperature for the experimental measurements is from (303.15 to 373.15) K in 10 K intervals. The solubility of CO_2 is determined by measuring the bubble-point pressure at a fixed temperature.

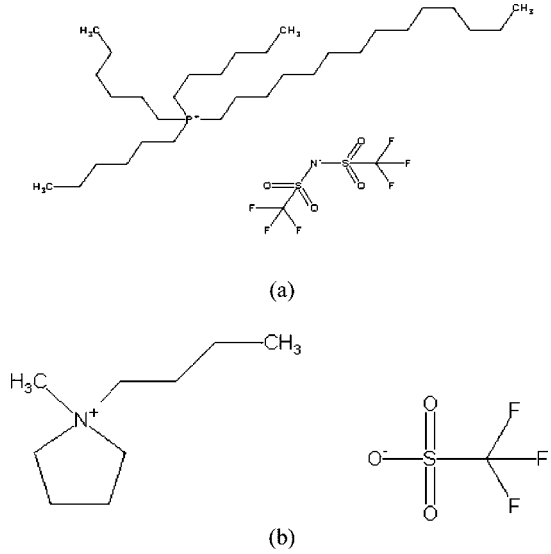

Figure 1. Chemical structure of ionic liquids: (a) [P14,6,6,6][Tf2N]; (b) [BMP][TfO].

Experimental Section

Chemicals. The ionic liquids [P14,6,6,6][Tf_2N] and [BMP][TfO] were purchased from Merck (Germany). The mass fraction purities of [P14,6,6,6][Tf_2N] and [BMP][TfO] are (99.5 and 99.6) %, respectively, and their residual chloride and water contents are below 100 ppm. The purity data by the high-performance liquid chromatography (HPLC) analysis were provided by the supplier. The chemical structures of [P14,6,6,6][Tf_2N] and [BMP][TfO] are shown in Figure 1. The ionic liquid sample was placed into the high-pressure variable-volume view cell for solubility measurement and evacuated by use of a vacuum pump at room temperature for several days.

* Corresponding author. Tel.:+82-2-705-8918; fax: +82-2-705-7899. E-mail: limjs@sogang.ac.kr.
[†] Sogang University.
[‡] Hannam University.

10.1021/je9005085
Published on Web 12/28/2009

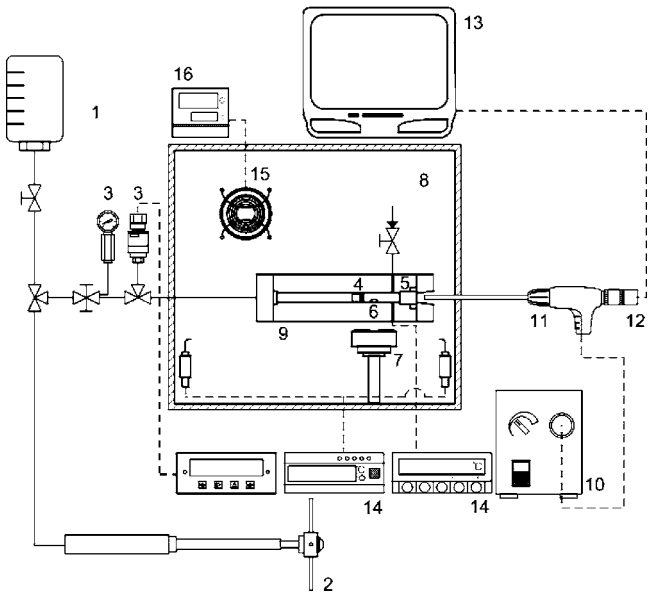

Figure 2. Schematic diagram of the experimental apparatus: (1) water for pressing; (2) pressure generator; (3) pressure gauge; (4) piston; (5) sapphire window; (6) magnetic bar; (7) stirrer; (8) air bath; (9) variable-volume view cell; (10) light source; (11) borescope; (12) CCD camera; (13) monitor; (14) temperature gauge; (15) heater; (16) heating controller.

Table 1. Critical Properties and Acentric Factor of Ionic Liquids Calculated from Modified Lydersen−Joback−Reid Method[16]

ionic liquid	M / g·mol^{-1}	T_b / K	T_c / K	P_c / MPa	ω
[P14,6,6,6][Tf_2N]	764.02	1310.56	1604.75	0.8513	0.7748
[BMP][TfO]	291.33	678.58	933.39	2.5859	0.6099

Coulometric Karl Fischer titration (Metrohm model 684) was performed on a sample of the evacuated ionic liquid. The water mass fraction was about $23 \cdot 10^{-6}$ for [P14,6,6,6][Tf2N] and $55 \cdot 10^{-6}$ for [BMP][TfO]. Carbon dioxide (CO_2) used for measurements was purchased from Deokyang Gas Co. (Korea) and had a high purity of 99.995 %. The ionic liquids and CO_2 gas were used without further purification.

Experimental Apparatus. The solubilities of CO_2 in the ionic liquids ([P14,6,6,6][Tf_2N] and [BMP][TfO]) were measured by using the high-pressure variable-volume view cell. Figure 2 shows a schematic diagram of the experimental apparatus for measuring the solubilities of CO_2 in ionic liquids. The experimental apparatus used in this work was the same as that used in our previous work.[11] The heart of the system is the high-pressure variable-volume view cell. The main feature of using the variable-volume cell apparatus is that the overall composition of the system is kept constant during the experiment. The cell has dimensions of 16 mm i.d. × 70 mm o.d. and an internal working volume of about 31 cm^3. A piston is placed inside the cell to change the cell volume. A pressure generator (High Pressure Equipment Co. model 50-6-15) is used to pressurize water and therefrom displace the piston. A change in the cell volume causes a change of the system pressure. A sapphire window is inserted into the view cell for visual observation of the interior of the cell. The system pressure was measured with a high-precision pressure gauge (Dresser Heise model CC-12-G-A-02B, ± 0.05 MPa accuracy) placed between the pressure generator and the view cell. The system temperature was measured to within ± 0.1 K by an RTD temperature probe inserted into the interior of the cell. A temperature-controlled forced-convection air bath was used to keep the system temperature constant. A visual observation of the interior of the cell through the sapphire window was made by a borescope (Olympus model R080-044-000-50) and a charge-coupled device (CCD) camera connected to a monitor. A magnetic stirring system was equipped under the cell body to mix the contents in the cell. A stirring bar in the cell was activated by a samarium−cobalt magnet located below the cell, and the magnet was driven by an electric motor.

Table 2. Solubility Data for the [P14,6,6,6][Tf2N] + CO_2 System

$x(CO_2)$	T / K	P / MPa	$x(CO_2)$	T / K	P / MPa	$x(CO_2)$	T / K	P / MPa
0.3603	293.65	0.53	0.7099	295.35	3.16	0.7928	293.35	5.51
	304.15	0.64		304.45	3.71		304.45	6.64
	313.85	0.72		315.05	4.29		313.45	7.92
	323.55	0.79		323.55	4.83		323.75	9.48
	333.55	0.9		333.15	5.43		335.15	11.28
	343.35	1.01		343.35	6.16		345.05	12.5
	354.25	1.13		353.45	6.88		354.55	13.87
	363.45	1.24		365.15	7.69		364.95	15.36
	373.15	1.37		372.65	8.20		373.95	16.62
0.5930	295.65	1.43	0.7254	294.05	3.53	0.8258	296.55	6.99
	303.85	1.65		303.35	4.03		303.15	8.27
	313.05	1.88		314.95	4.79		313.35	10.45
	323.75	2.13		324.05	5.55		322.95	12.47
	333.45	2.35		333.85	6.25		334.15	14.72
	343.35	2.61		343.15	7.00		344.05	16.60
	353.65	2.88		354.25	7.87		355.25	18.64
	363.15	3.13		363.35	8.63		363.45	20.36
	373.65	3.39		373.65	9.42		373.65	22.20
0.6309	296.05	2.11	0.7406	294.95	4.03			
	304.35	2.43		304.25	4.54			
	313.35	2.74		313.85	5.53			
	324.35	3.16		323.75	6.39			
	334.65	3.58		333.55	7.24			
	344.65	3.99		343.25	8.13			
	354.45	4.40		355.45	9.16			
	364.15	4.78		364.65	10.02			
	374.25	5.19		374.55	10.91			
0.6831	296.35	2.63	0.7611	296.95	5.05			
	304.25	2.93		305.05	5.76			
	313.75	3.44		314.55	6.67			
	323.25	3.92		324.15	7.73			
	333.85	4.42		334.15	8.81			
	344.55	4.89		344.05	9.95			
	354.35	5.43		355.15	11.16			
	363.75	5.98		364.15	12.19			
	375.35	6.60		373.55	13.20			

Experimental Procedure. The ionic liquid sample was loaded to the high-pressure variable-volume view cell.The amount of sample was about (8 to 9) g. It makes adequate space to agitate the stirring bar in the variable view cell. The piston, stirring bar, and sapphire window are inserted into the variable view cell. A piston makes the space inside the cell by pressure generator that is used to pressurize water. We can observe inside the cell though the sapphire window. To remove any entrapped air present in the cell and any dissolved gas and water in the ionic liquid, the cell was evacuated by vacuum pump at room temperature for several days before experiment. Once the vapor space of the system was fully evacuated, a known amount of CO_2 was loaded into cell. The exact amount of CO_2 gas introduced into the cell was determined by weighing the CO_2 sample cylinder before and after loading using a balance (Precisa model 1212 M) with an accuracy of ± 1 mg. To prevent any loss of CO_2 gas in the feed line during loading, the CO_2 gas in the feed line was recovered back into the CO_2 sample cylinder by dipping the cylinder into a Dewar flask filled with liquid nitrogen. The uncertainties in measuring ionic liquid and CO_2 are (0.2 and 2) mg, respectively. The uncertainty analysis for the composition measurement for each component was performed in accordance with the International Organization of

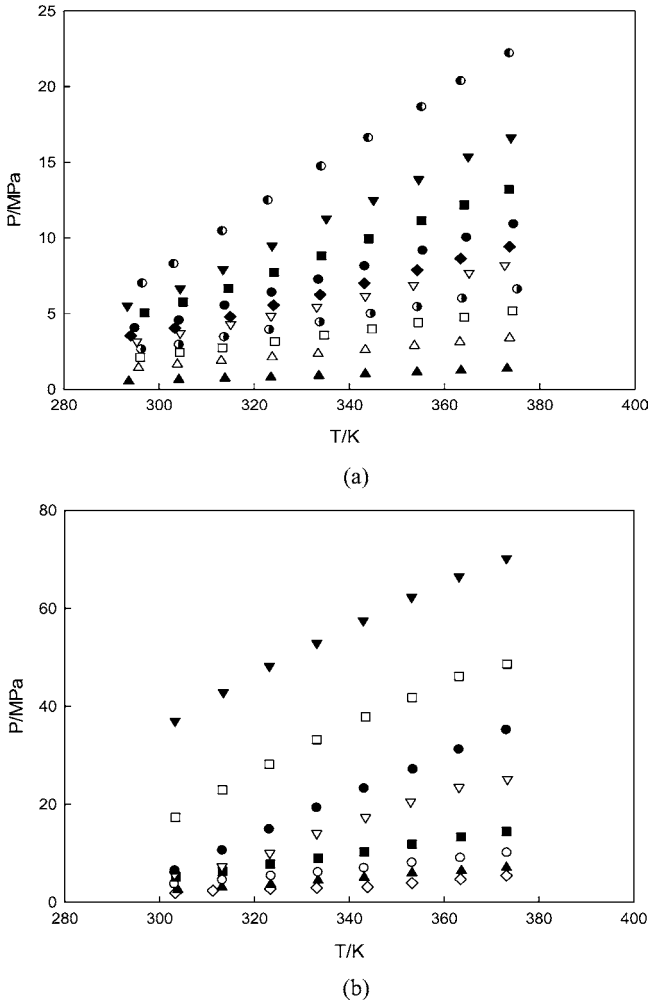

Figure 3. $P-T$ graph of CO_2 solubilities of the CO_2 + ionic liquid system. (a) CO_2 + [P14,6,6,6][Tf2N] (CO_2 mole fraction): ▲, 0.3603; △, 0.5930; □, 0.6309; ◑, 0.6831; ▽, 0.7099; ◆, 0.7254; ●, 0.7406; ■, 0.7611; ▼, 0.7928; and ◐, 0.8258. (b) CO_2 + [BMP][TfO]: ◇, 0.2584; ▲, 0.3118; ○, 0.3877; ■, 0.4623; ▽, 0.5697; ●, 0.6216; □, 0.6651; and ▼, 0.7058.

Standardization (ISO) guideline,[12] and it was analyzed within ± 0.005 mol fraction for each component. The mole fraction of CO_2 in the ionic liquid was calculated on the basis of a known amount of CO_2. The ionic liquid and CO_2 were agitated by a stirring bar to make a single phase. As the pressure increased, CO_2 and the ionic liquid became a homogeneous phase. After the pressure was slowly reduced until the first CO_2 bubble was observed from the solution. At this moment, we measured the pressure of the cell, and we regarded this pressure as the bubble-point pressure at a fixed CO_2 mole fraction and temperature. The pressure reduction rates for the determinations of the bubble-point pressure ranged approximately from 0.05 MPa·s^{-1} for the highest bubble-point pressure case to 0.001 MPa·s^{-1} for the lowest bubble-point pressure case. The reduction rate was so slow that the effect of the rate on the results of the bubble-point pressure was not observed. After one set of experiment (from (303.15 to 373.15) K) was finished at a fixed CO_2 mole fraction, more CO_2 was charged into the cell, and a CO_2 mole fraction of a new set of the experimental system was recalculated. All of the other experiments having increasing CO_2 mole fractions were performed in this manner. Every measurement was repeated more than three times at each temperature to obtain accurate data. The uncertainty of the temperature measurement was ± 0.1 K, and the bubble-point pressure measurement was ± 0.01 MPa.

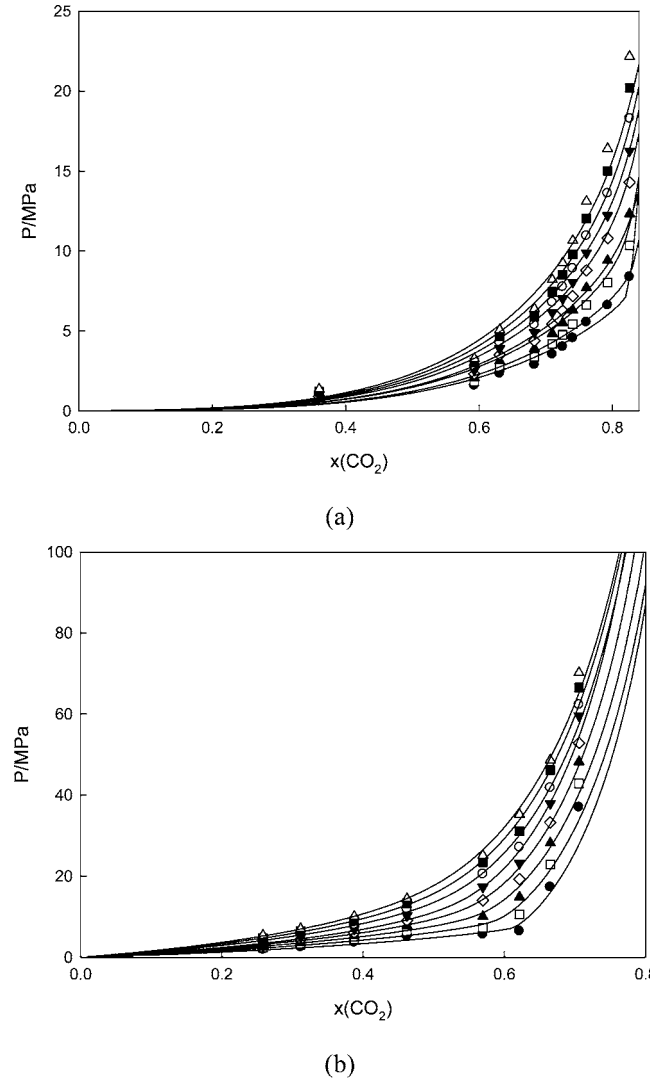

Figure 4. $P-x_1$ graph of CO_2 solubilities of the CO_2 + ionic liquid system: (a) [P14,6,6,6][Tf2N] and (b) [BMP][TfO]. ●, 303.15 K; □, 313.15 K; ▲, 323.15 K; ◇, 333.15 K; ▼, 343.15 K; ○, 353.15 K; ■, 363.15 K; and △, 373.15 K; —, calculated by PR-EoS.[13]

Modeling

The experimental (CO_2 + ionic liquid) data were correlated with the Peng−Robinson equation of state (PR-EoS).[13]

$$P = \frac{RT}{V-b} - \frac{a(T)}{V(V-b)+b(V-b)} \quad (1)$$

The mixture parameters in the ionic liquid phase are calculated from following four mixing rules:

$$a = \sum_i \sum_j x_i x_j a_{ij} \quad (2)$$

$$a_{ij} = (a_{ii}a_{jj})^{1/2}(1-k_{ij}) \quad (3)$$

$$b = \sum_i \sum_j x_i x_j b_{ij} \quad (4)$$

$$b_{ij} = \left(\frac{b_i + b_j}{2}\right)(1-l_{ij}) \quad (5)$$

In eqs 3 and 4, l_{ij} and k_{ij} are the binary interaction parameters. In eq 4, $b_{ii} = b_i$ and $b_{jj} = b_j$.

$$a_{ii} = \frac{0.457235R^2T_{ci}^2}{P_{ci}}\left[1 + (0.37464 + 1.54226\omega_i - 0.26992\omega_i^2)\left(1 - \sqrt{\frac{T}{T_{ci}}}\right)\right]^2 \quad (6)$$

$$b_i = \frac{0.077796RT_{ci}}{P_{ci}} \quad (7)$$

To calculate the parameters of the PR-EoS, critical temperature (T_c), critical pressure (P_c), and the acentric factor (ω) of both components, CO_2 and ionic liquids, were needed. Those properties of CO_2 are easily obtained from literature;[14] however, those of ionic liquids are not available. Therefore, critical properties of ionic liquids have to be estimated. In this work, to estimate the critical properties of ionic liquids, we used the modified Lydersen−Joback−Reid method[15,16] which is a group contribution method and is known to give relatively good results especially for the molecules having high molecular weights.[16]

$$T_b/\mathrm{K} = 198.2 + \sum n\Delta T_{bM} \quad (8)$$

$$T_c/\mathrm{K} = \frac{T_b}{0.5703 + 1.0121\sum n\Delta T_M - (\sum n\Delta T_M)^2} \quad (9)$$

$$P_c/\mathrm{MPa} = \frac{M}{(0.2573 + \sum n\Delta P_M)^2} \quad (10)$$

where M is the molecular weight of the ionic liquid. The groups considered for the modified Lydersen−Joback−Reid method are presented in the literature.[15]

The acentric factor is calculated as[15]

$$\omega = \frac{(T_b - 43)(T_c - 43)}{(T_c - T_b)(0.7T_c - 43)} \log\left[\frac{p_c}{p_b}\right] - \frac{(T_c - 43)}{(T_c - T_b)} \log\left[\frac{p_c}{p_b}\right] + \log\left[\frac{p_c}{p_b}\right] - 1 \quad (11)$$

Acentric factor is calculated by critical properties and normal boiling temperature (T_b for $P_b = 0.1$ MPa). All of the calculated critical properties, the normal boiling temperature, and acentric factors of ionic liquids are listed in Table 1.

Table 3. Solubility Data for the [BMP][TfO] + CO_2 System

	T	P		T	P
$x(CO_2)$	K	MPa	$x(CO_2)$	K	MPa
0.2583	303.35	1.88	0.5697	303.15	5.62
	311.25	2.35		313.15	7.27
	323.35	2.71		323.25	10.00
	333.15	2.92		333.15	14.00
	343.85	3.10		343.45	17.30
	353.25	3.91		352.95	20.50
	363.45	4.71		363.15	23.46
	373.15	5.43		373.35	25.12
0.3118	303.85	2.49	0.6216	303.25	6.45
	313.15	3.06		313.25	10.55
	323.45	3.62		323.15	14.87
	333.45	4.41		333.15	19.24
	343.15	5.03		343.15	23.20
	353.25	5.95		353.45	27.11
	363.65	6.39		363.15	31.16
	373.15	7.05		373.15	35.17
0.3877	303.15	3.66	0.6651	303.35	17.30
	313.25	4.51		313.25	22.90
	323.55	5.34		323.15	28.17
	333.45	6.08		333.15	33.20
	343.15	6.95		343.45	37.88
	353.25	8.06		353.25	41.80
	363.45	9.02		363.15	46.15
	373.25	10.09		373.25	48.65
0.4623	303.45	5.16	0.7058	303.25	36.99
	313.25	6.29		313.45	42.86
	323.35	7.79		323.15	48.21
	333.45	9.00		333.15	52.92
	343.15	10.27		342.95	59.53
	353.25	11.84		353.15	62.30
	363.55	13.34		363.15	66.50
	373.15	14.44		373.15	70.20

Table 4. Binary Interaction Parameters for the Ionic Liquids System

T	[P14,6,6,6][Tf2N]		[BMP][TfO]	
K	k_{12}	l_{12}	k_{12}	l_{12}
303.15	0.0729	0.0660	0.0834	0.0253
313.15	0.0710	0.0677	0.0858	0.0227
323.15	0.0688	0.0702	0.0907	0.0237
333.15	0.0664	0.0731	0.0971	0.0265
343.15	0.0641	0.0764	0.1059	0.0329
353.15	0.0619	0.0799	0.1063	0.0283
363.15	0.0592	0.0834	0.1111	0.0293
373.15	0.0562	0.0863	0.1153	0.0310

Table 5. Average Absolute Deviation (AAD %) between Experimental Data and Calculated Value for the [P14,6,6,6][Tf2N] + CO_2 and [BMP][TfO] + CO_2 System

T	AAD %[a]	
K	[P14,6,6,6][Tf2N]	[BMP][TfO]
303.15	11.82	8.44
313.15	11.99	11.86
323.15	12.09	9.43
333.15	12.26	7.45
343.15	12.38	7.38
353.15	12.59	5.33
363.15	12.81	2.87
373.15	13.33	2.95
average	12.41	6.96

[a] Average absolute deviation in percentage:

$$\mathrm{AAD}\,\% = \frac{1}{N}\sum_{i=1}^{N}\frac{|P_i^{calc} - P_i^{exp}|}{P_i^{exp}} \cdot 100 \quad (N = \text{number of data})$$

Results and Discussion

In this work, the solubility of carbon dioxide in [P14,6,6,6][Tf2N] was measured in the temperature range from (293.15 to 373.15) K in 10 K intervals. The experimental results are given in Table 2. Figures 3a and 4a show their bubble-point pressures versus the temperature and CO_2 mole fraction, respectively. High-pressure phase behavior of carbon dioxide in [BMP][TfO] was measured in the temperature range from (303.15 to 373.15) K in 10 K intervals. The experimental results are given in Table 3. Figures 3b and 4b also show their bubble-point pressures versus the temperature and CO_2 mole fraction, respectively. As can be seen in Figure 3, the bubble-point pressure increases linearly with increasing temperature at a fixed CO_2 mole fraction. It means that, at a fixed pressure, the solubility of CO_2 in ionic liquid decreases with increasing temperature. At a fixed CO_2 mole fraction, the CO_2 solubility in ionic liquid is dramatically affected by temperature. Figure 4 shows that, as the CO_2 mole fraction increases, the bubble-point pressures increase dramatically. So the slope of the solubility pressure with temperature increased steeply with increasing CO_2 mole fraction, and the bubble-point pressures increased with increasing CO_2 mole fraction at a fixed temperature.

Calculated binary interaction parameters from (303.15 to 373.15) K in 10 K intervals for each system are given in Table 4. The calculated results from the PR-EoS with mixing rules are illustrated in Figure 4 along with the experimental data. The correlation model successfully predicts the solubility pressure data at a lower mole fraction of CO_2. But as the mole fraction of CO_2 increases, the deviation between experimental data and calculated results becomes larger. Deviations between experi-

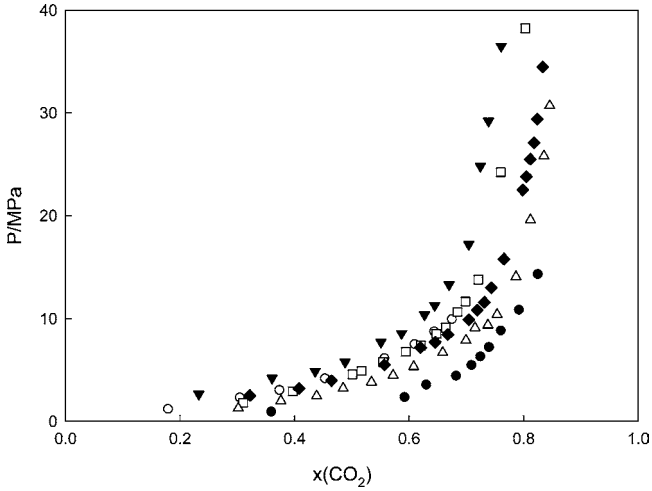

Figure 5. Comparison of the $P-x_1$ graph of CO_2 solubilities in the [Tf2N] based ionic liquid systems at 333.15 K: ●, [P14,6,6,6][Tf2N] (this work); △, [C_8-mim][Tf2N];[12] ◆, [C_6-mim][Tf2N];[12] □, [C_4-mim][Tf2N];[12] ▼, [C_2-mim][Tf2N];[11] and ○, [hmim][Tf2N].[17]

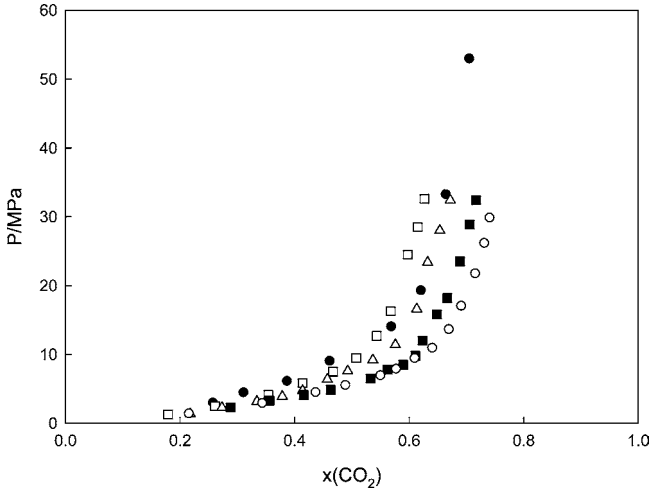

Figure 6. Comparison of the $P-x_1$ graph of CO_2 solubilities in the [TfO] based ionic liquid systems at 333.15 K: ○, [C_8-mim][TfO];[24] ■, [C_6-mim][TfO];[24] △, [C_4-mim][TfO];[24] ●, [BMP][TfO] (this work); and □, [C_2-mim][TfO].[24]

mental and calculated values are shown in Table 5. We calculate the average absolute deviation in percentage (AAD %) for each system. The average value of the AAD % of [P14,6,6,6][Tf2N] was two times higher than that of [BMP][TfO]. As the temperature increases, the AAD % values of [BMP][TfO] decrease, whereas the AAD % values of [P14,6,6,6][Tf2N] are similar in all temperature ranges.

Recently, a number of papers have been published about the solubility of CO_2 in ionic liquids: CO_2 + [C_n-mim][Tf2N],[11] CO_2 + [hmin][Tf2N],[17] CO_2 + [bmim][PF_6],[18] CO_2 + [omim][BF_4],[19] CO_2 + [bmim][BF_4],[20] CO_2 + [hmim][BF_4],[21] CO_2 + [hmim][PF_6],[21] CO_2 + [C_8mim][PF_6], CO_2 + [bmim][NO_3], CO_2 + [C_8mim][BF_4], CO_2 + [*N*-buty][BF_4], CO_2 + [emim][$EtSO_4$],[23] and CO_2 + [C_n-mim][TfO].[24] Figure 5 compares the solubility data for the [P14,6,6,6][Tf2N] + CO_2, [hmin][Tf2N] + CO_2, and [C_n-mim][Tf2N] + CO_2 systems at 333.15 K. It shows the effect of different cations on the solubility of CO_2 in the [Tf2N] anion-based ionic liquids. All of the ionic liquids in Figure 5 were almost same at under $0.5x_1$. But at high x_1, the experimental values show different aspects. The [P14,6,6,6][Tf2N] + CO_2 system has lower bubble-point pressures than other systems in the entire mole fraction. It means

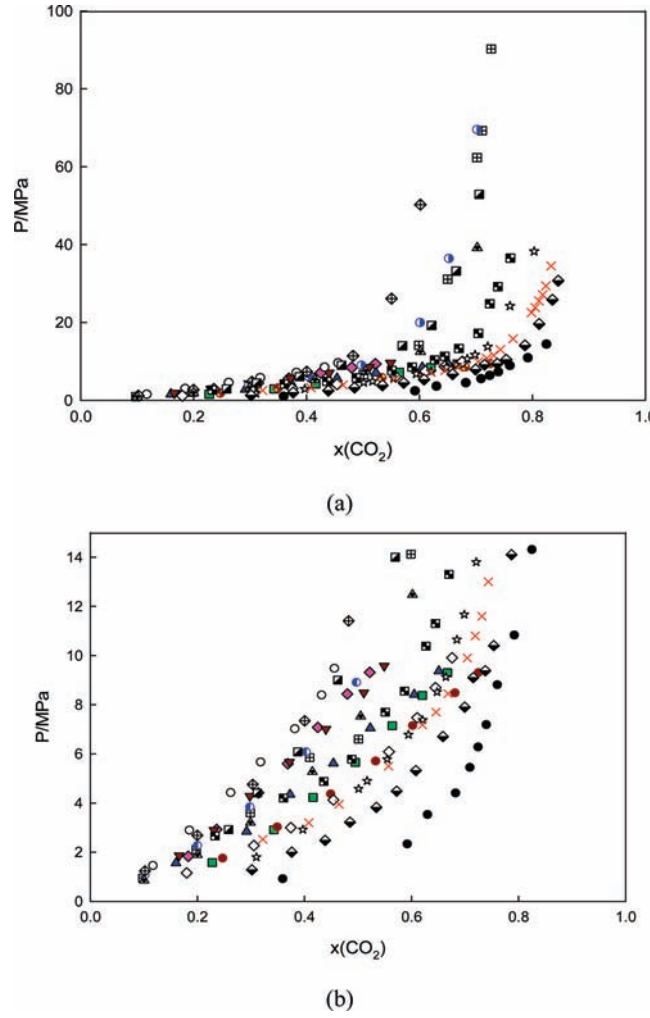

Figure 7. Comparison of the $P-x(CO_2)$ graph of CO_2 solubilities in 17 different ionic liquids at 333.15 K: green ■, [bmim][PF_6];[18] yellow and dark red ●, [C_8mim][PF_6]; ◇, [bmim][NO_3]; blue ▲, [C_8mim][BF_4]; dark red ▼, [*N*-buty][BF_4]; ○, [emim][$EtSO_4$];[23] ⊞, [hmim][PF_6];[22] blue ◑, [hmim][BF_4];[21] tilted square with cross, [bmim][BF_4];[20] ⟁, [omim][BF_4];[19] ●, [P14,6,6,6][Tf2N]; ◪, [BMP][TfO]; ◇, [hmin][Tf2N];[17] ⊞ with solid upper left and lower right windows, [C_2-mim][Tf2N];[11] ☆, [C_4-mim][Tf2N];[11] red ×, [C_6-mim][Tf2N];[11] tilted square with solid bottom half, [C_8-mim][Tf2N].[11] (b) Enlarged graph for a; the symbols are same as a.

that the solubility of CO_2 is higher in [P14,6,6,6][Tf2N] than in [hmin][Tf2N] and [C_n-mim][Tf2N]. Figure 5 also illustrates that the solubility of CO_2 increases as the alkyl group chain length increases. This tendency is similar with a previous result in the literature.[17,20] As the CO_2 mole fraction increases, the bubble-point pressures increase dramatically. Figure 6 compares the solubility data for the [BMP][TfO] + CO_2 and [C_n-mim][TfO] + CO_2 system at 333.15 K. It shows the effect of different cations on the solubility of CO_2 in the [TfO] anion-based ionic liquids. As shown in this figure, at a lower mole fraction of CO_2, the solubility of CO_2 in different ionic liquids is almost the same. But when over $0.5x_1$, the solubility of CO_2 shows a completely different tendency. Figure 6 also shows that CO_2 is the most soluble in [C_8-min][TfO] among those [TfO] anion-based ionic liquids. Figure 7 compares the all of the solubility data which have been published in the literature. As can be seen in this figure, CO_2 is most soluble in [P14,6,6,6][Tf2N]. An enlarged $P-x_1$ graph of Figure 7a is shown in Figure 7b.

Conclusions

Experimental results for the solubility of CO_2 in the ionic liquids [P14,6,6,6][Tf2N] and [BMP][TfO] were observed from

(303.15 to 373.15) K in 10 K intervals. The solubility of CO_2 in ionic liquids was measured by using a high-pressure variable-volume view cell. A normal boiling temperature, acentric factor, and critical properties of ionic liquids were estimated by the modified Lydersen−Joback−Reid method. The PR-EoS and mixing rules were used to calculate the solubility pressure. At a lower mole fraction of CO_2, CO_2 shows very high solubilities in the ionic liquids. The bubble-point pressure increases sharply at a high mole fraction of CO_2 and increases linearly with increasing temperature at a fixed mole fraction of CO_2.

Literature Cited

(1) Anthony, J. L.; Maginn, E. J.; Brennecke, J. F. Solubilities and thermodynamic properties of gases in the ionic liquid 1-n-butyl-3-methylimidazolium hexafluorophosphate. *J. Phys. Chem. B* **2002**, *106*, 315–320.

(2) Gota, I.; Gonzalez-Olmos, R.; Iglesias, M.; Medina, F. New short aliphatic chain ionic liquids: Synthesis, Physical properties and catalytic activity in aldol condensation. *J. Phys. Chem. B* **2007**, *111*, 12468–12477.

(3) Renken, A.; Hessel, V.; Lob, P.; Miszczuk, R.; Uerdingen, M.; Kiwiminsker, L. Ionic liquid synthesis in a microstructured reactor for process intensification. *Chem. Eng. Process.* **2007**, *46*, 840–845.

(4) Zein El Abedin, S.; Pölleth, M.; Meiss, S. A.; Janek, J.; Endres, F. Ionic liquids as green electrolytes for the electrodeposition of nonmaterials. *Green Chem.* **2007**, *9*, 549–553.

(5) Cheek, G. T.; O'Grady, W. E.; Zein El Abedin, S.; Moustafa, E. M.; Endres, F. Studies on the electrodeposition of magnesium in ionic liquids. *J. Electrochem. Soc.* **2008**, *155*, D91–D95.

(6) Bennett, M. D.; Leo, D. J. Ionic liquids as stable solvents for ionic polymer transducers. *Sens. Actuators, A* **2004**, *115*, 79–90.

(7) Anthony, J. L.; Maginn, E. J.; Brennecke, J. F. Solution thermodynamics of imidazolium-based ionic liquids and water. *J. Phys. Chem. B* **2001**, *105*, 10942–10949.

(8) Visser, A. E.; Swatloski, R. P.; Reichert, W. M.; Griffin, S. T.; Rogers, R. D. Traditional extractants in nontraditional solvents: groups 1 and 2 extraction by crown ethers in room-temperature ionic liquids. *Ind. Eng. Chem. Res.* **2000**, *39*, 3596–3604.

(9) Ari, Y.; Sako, T.; Takebayashi, Y. *Supercritical Fluids: Molecular Interactions, Physical Properties, and New Applications*; Springer: New York, 2001.

(10) Blanchard, L. A.; Brennecke, J. F. Recovery of Organic Products from Ionic Liquids Using Supercritical Carbon Dioxide. *Ind. Eng. Chem. Res.* **2001**, *40*, 287–292.

(11) Sin, E.-K.; Lee, B.-C.; Lim, J. S. High-pressure solubilities of carbon dioxide in ionic liquids: 1-Alkyl-3-methylimidazolium bis(trifluoromethylsulfonyl)imide. *J. Supercrit. Fluids* **2008**, *45*, 282–292.

(12) *Guide to the Expression of Uncertainty in Measurement International Organization of Standardization (ISO)*; ISO: Geneva, Switzerland, 1995.

(13) Peng, D. Y.; Robinson, D. B. A New Two-Constant Equation of State. *Ind. Eng. Chem. Fundam.* **1976**, *15*, 59.

(14) McLinden, M. O.; Klein, S. A.; Lemmoon E. W.; Peskin, A. P. *Thermodynamic Properties of Refrigerants and Refrigerant Mixtures Database (REFPROP)*, version 6.01; NIST: Gaithersburg, MD, 1998.

(15) Valderrama, J. O.; Sanga, W. W.; Lassús, J. A. Critical properties, normal boiling temperature, and acentric factor of another 200 ionic liquids. *Ind. Eng. Chem. Res.* **2008**, *47*, 1318–1330.

(16) Valderrama, J. O.; Robles, P. A. Critical properties, normal boiling temperatures, and acentric factors of fifty ionic liquids. *Ind. Eng. Chem. Res.* **2007**, *46*, 1338–1344.

(17) Kumelan, J.; Kamps, Á. P.; Tuma, D.; Maurer, G. Solubility of CO_2 in the ionic liquid [hmim][Tf2N]. *J. Chem. Thermodyn.* **2006**, *38*, 1396–1401.

(18) Shariati, A.; Gutkowski, K. I.; Peters, C. J. Comparison of the phase behavior of some selected binary systems with ionic liquids. *AIChE J.* **2005**, *51*, 1532–1540.

(19) Gutkowski, K. I.; Shariati, A.; Peters, C. J. High-pressure phase behavior of the binary ionic liquid system 1-octyl-3-methylimidazolium tetrafluoroborate +carbon dioxide. *J. Supercrit. Fluids* **2006**, *39*, 187–191.

(20) Kroon, M. C.; Shariati, A.; Costantini, M.; van Spronsen, J.; Witkamp, G.-J.; Sheldon, R. A.; Peters, C. J. High-pressure phase behavior of systems with ionic liquids: Part V. The binary system carbon dioxide + 1-Butyl-3-methylimidazolium tetrafluoroborate. *J. Chem. Eng. Data* **2005**, *50*, 173–176.

(21) Costantini, M.; Toussaint, V. A.; Shariati, A.; Peters, C. J.; Kikic, I. High-pressure phase behavior of systems with ionic liquids: Part IV. Binary system carbon dioxide + 1-hexyl-3-methylimidazolium tetrafluoroborate. *J. Chem. Eng. Data* **2005**, *50*, 52–55.

(22) Shariati, A.; Peters, C. J. High-pressure phase behavior of systems with ionic liquids Part III. The binary system carbon dioxide + 1-hexyl-3-methylimidazolium hexafluorophosphate. *J. Supercrit. Fluids* **2004**, *30*, 139–144.

(23) Blanchard, L. A.; Gu, Z.; Brennecke, J. F. High-pressure phase behavior of ionic liquid/CO_2 systems. *J. Phys. Chem. B* **2001**, *105*, 2437–2444.

(24) Sin, E.-K.; Lee, B.-C. High-pressure phase behavior of carbon dioxide with ionic liquids: 1-Alkyl-3-methylimidazolium trifluoromethanesulfonate. *J. Chem. Eng. Data* **2008**, *53*, 2728–2734.

Received for review June 16, 2009. Accepted December 14, 2009. This research was supported by a Sogang University Research Grant in 2008.

JE9005085